

# Bifurcation structures and transient chaos in a four-dimensional Chua model

Anderson Hoff, Denilson T. da Silva, Cesar Manchein, Holokx A. Albuquerque\*

*Departamento de Física, Universidade do Estado de Santa Catarina, 89219-710 Joinville, Brazil*

---

## Abstract

A four-dimensional four-parameter Chua model with cubic nonlinearity is studied applying numerical continuation and numerical solutions methods. Regarding numerical solution methods, its dynamics is characterized on Lyapunov and isoperiodic diagrams and regarding numerical continuation method, the bifurcation curves are obtained. Combining both methods the bifurcation structures of the model were obtained with the possibility to describe the *shrimp*-shaped domains and their endoskeletons. We study the effect of a parameter that controls the dimension of the system leading the model to present transient chaos with its corresponding basin of attraction being riddled.

**Keywords:** Four-dimensional model, Bifurcation curves, Transient chaos, Shrimps.

\*Corresponding author. Tel.: +55 47 4009 7721; fax: +55 47 4009 7940. Email: holokx.albuquerque@udesc.br

---

## 1. Introduction

In dynamical systems a bifurcation structure is a change of qualitative behavior when control parameters are varied. Recently, a plethora of bifurcation structures is being reported in many types of discrete- and continuous-time nonlinear dynamical systems, when two or more control parameters are varied [1–15]. In such works and references therein a common feature observed in the parameter-planes is the occurrence of isoperiodic stable structures, often namely *shrimp*-shaped domains (SSD's), with a variety of bifurcation cascades and organization rules. In the last years, many works [10, 16–19] use numerical continuation methods to unveil in more details the bifurcation structures in the parameter-planes of low order dissipative systems. In particular, the authors of a recent Letter [10] use numerical continuation techniques to study in details a periodic domain in the biparametric-space of the two-dimensional Hénon map. In that work, the authors claimed that using continuation methods is more feasible to analyze the delicate bifurcation structures for both nonlinear differential equations and maps, than use shooting methods.

Regarding the Chua circuit model [1, 3, 20–22], a paradigm of chaotic behavior, in the last four decades an enormous quantity of published papers report the

rich dynamics that this circuit presents. The canonical Chua model consists of three coupled first-order ordinary differential equations with a piecewise linear function. Other smooth nonlinear functions are also used [20, 23, 24]. In all these three-dimensional Chua models the bifurcation structures in the parameter-planes present different types of roles and organizations. Based on the canonical three-dimensional Chua model, high-dimensional versions can be constructed introducing feedback controllers [3, 25], *i.e.*, adding another variables in the model. In this configuration, the high-dimensional model can present more complex dynamics, as hyperchaos [3].

Our main goal in this Letter is to apply numerical continuation methods [26] in addition with numerical solution methods to unveil the bifurcation structures in two-dimensional parameter-spaces, and the endoskeletons of SSD's, in a high-dimensional continuous-time nonlinear model. In this work we show that the endoskeleton of a SSD is formed by four main bifurcation curves: two saddle-node curves with one cusp point and two intersected period-doubling curves. These four curves delimit the lowest-period of the structure. Another remarkable observation is the presence of transient chaos in the two-dimensional parameter-spaces of the model. As far as we know, the work here reported is one of the first to combine both numerical continuation and numerical solution methods in high-dimensional continuous-time nonlinear model to discuss the bifur-

---

*Email addresses:* hoffande@gmail.com (Anderson Hoff), cesar.manchein@udesc.br (Cesar Manchein)

cation structures presented by the model.

This paper is organized as follows: In Section 2 we present the model with a brief description of the employed methods. In Section 3 we present the numerical results with some discussions, and in Section 4 we present the conclusions of this work.

## 2. The four-dimensional model

The nonlinear model studied has the origin in the canonical three-dimensional three-parameters Chua model with cubic nonlinearity, adding a controller variable  $w$  and a fourth parameter  $d$  as proposed in a recent paper [25]. The nonlinear equations are

$$\begin{aligned}\dot{x} &= \frac{dx}{dt} = a(y + 0.2(x - x^3)), \\ \dot{y} &= \frac{dy}{dt} = bx - y + z + w, \\ \dot{z} &= \frac{dz}{dt} = -cy + w, \\ \dot{w} &= \frac{dw}{dt} = -dy,\end{aligned}\tag{1}$$

where  $x$ ,  $y$ ,  $z$ , and  $w$  are the variables, that represent the voltages in the real circuit [25],  $a$ ,  $b$ ,  $c$ , and  $d$  are the parameters, related to combinations of resistors and capacitors in the real circuit. Such system is a four-parameter model and the parameter  $d$  controls the extra-dimension, once that if  $d$  vanish, the last differential equation of the system (1) vanish, too. Therefore, if we initialize the system (1) with the initial conditions  $(x, y, z, w) = (0.1, 0.1, 0.1, 0.0)$ , we will have the canonical three-dimensional Chua system, as reported in the Refs. [1, 20–22, 24].

It is well known that for a four-dimensional system, the Lyapunov spectrum has four values of exponent,  $(\lambda_1, \lambda_2, \lambda_3, \lambda_4)$ , one value for each direction of the flow. Here, we use the largest exponent of the spectrum to study in the parameter-spaces (henceforth Lyapunov diagrams) the behaviors of the system (1) identifying colors to the exponent values. For this purpose, the four-dimensional Lyapunov diagram,  $a \times b \times c \times d$ , is sliced in the following parameter combinations:  $a \times b$  with  $c$  and  $d$  fixed,  $a \times c$  with  $b$  and  $d$  fixed,  $b \times c$  with  $a$  and  $d$  fixed,  $a \times d$  with  $b$  and  $c$  fixed,  $b \times d$  with  $a$  and  $c$  fixed, and  $c \times d$  with  $a$  and  $b$  fixed. To obtain the Lyapunov spectra, the model is numerically solved by the Runge-Kutta method with fixed time step equal to  $1.0 \times 10^{-2}$  and  $5.0 \times 10^5$  integrated steps to obtain the exponent spectrum via the algorithm proposed in [27] for each

parameter pair discretized in a grid of  $500 \times 500$  values. Therefore, we obtain  $2.5 \times 10^5$  Lyapunov exponent spectra for each parameter pair.

On the other hand, the bifurcation curves are obtained by continuation methods, using a properly continuation package for continuous-time systems, as MATCONT [26], which is a standard tool for numerical bifurcation analysis. Here we superimpose the bifurcation curves of Hopf, saddle-node, and period-doubling on the Lyapunov diagrams to unveil some bifurcation structures presented by the system (1) in the parameter-space.

The parameter-space of periods (henceforth isoperiodic diagrams), is used to corroborate the period-doubling and saddle-node bifurcation structures presented by the system (1). The periods are obtained by the maxima of the time-series for a given set of parameters, as done in Ref. [9]. To evaluate the period we use the Runge-Kutta method with variable time step, removing a transient time equal to  $5 \times 10^6$  and using more  $1 \times 10^6$  iterations to find the period with a precision of  $1 \times 10^{-3}$ . The parameter pairs were discretized in a grid of  $1200 \times 1200$  values.

## 3. Results

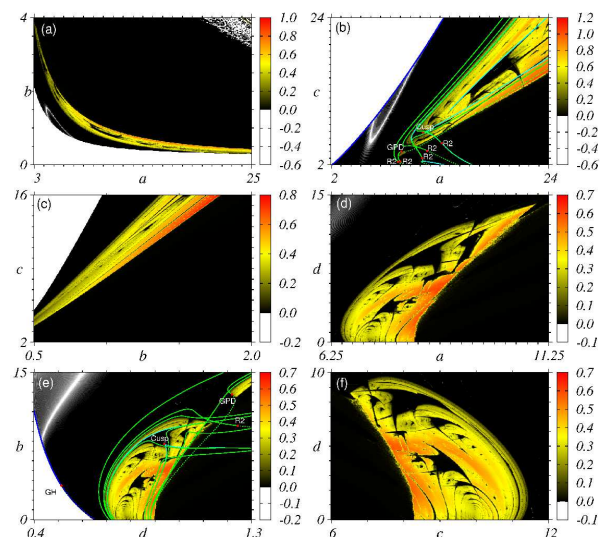


Figure 1: (Color online) Lyapunov diagrams for the largest exponent of the Lyapunov spectrum codified by colors, as the color bars at the right side of each diagram, for the six combinations of parameters of the system (1). (a)  $(a \times b)$  with  $c = 12.5$  and  $d = 5.0$ , (b)  $(a \times c)$  with  $b = 0.55$  and  $d = 10.0$ , (c)  $(b \times c)$  with  $a = 7.0$  and  $d = 1.0$ , (d)  $(a \times d)$  with  $b = 0.88$  and  $c = 8.5$ , (e)  $(b \times d)$  with  $a = 8.0$  and  $c = 8.5$ , and (f)  $(c \times d)$  with  $a = 8.0$  and  $b = 0.88$ . The blue, green, and cyan curves in (b) and (e) are Hopf, period-doubling, and saddle-node bifurcation curves, respectively.

Figure 1 shows the Lyapunov diagrams for six slices of the four-dimensional parameter-space of the system (1). In the diagrams the largest of the Lyapunov spectrum is codified in colors following the color bars at the right side. White, black and yellow/red regions in the diagrams refer to the equilibrium points, periodic points, and chaotic behaviors of system (1), respectively. In these diagrams, an abundant presence of periodic structures (black regions) immersed in chaotic regions (yellow/red regions) can be observed, as well as large regions of equilibrium points (white regions). Some periodic structures observed in Fig. 1 are reported in others works for different types of systems, indicating that these structures are general, moreover, these structures are organized in specific directions on the Lyapunov diagrams. Some of these structures are known by SSD's [28]. In (b) and (e) the Hopf, period-doubling, and saddle-node curves, blue, green, and cyan lines, respectively, are superimposed. The Hopf curve delimits the equilibrium points (white region) to limit cycles (black region) bifurcations, the period-doubling curves delimit the regions where occur a doubling of the limit cycles, and the saddle-node curve delimits the points where a chaotic attractor disappears and a stable periodic attractor is created. The solid and dashed green lines are stable and unstable period-doubling curves, respectively. The red points R2 and GPD are: 1:2 resonance point where two eigenvalues are equal to  $-1$ , and generalized period-doubling point where one eigenvalue is equal to  $-1$  and the normal form coefficient is null, respectively, and denote the location of stability loss of the period-doubling curves. The bifurcation curves shown in Figs. 1(b) and 1(e) reveal the bifurcation structures in a two-dimensional parameter-space and as can be seen in such figures, the curves delimit the boundaries between the stable points and chaotic domains, as well as the endoskeleton of the SSD's. The bifurcation curves for the other Lyapunov diagrams in Fig. 1 were omitted by sake of simplicity, because the bifurcation structures in these diagrams not present new information of those presented in the exemplary cases of Figs. 1(b) and 1(e).

To present, in more details, the bifurcation structures of the system (1), we show in Figs. 2 and 3 the Lyapunov and isoperiodic diagrams for the  $a \times c$  plane with  $b = 0.55$  and  $d = 10.0$ , and for  $b \times d$  plane with  $a = 8.0$  and  $c = 8.5$ , respectively. These diagrams are amplifications of Figs. 1(b) and 1(e). The period-doubling and saddle-node bifurcation curves, in green and cyan, respectively, obtained by numerical continuation method, are superimposed on the Lyapunov diagrams and reveal the set of points in the parameter-space where period-

doublings and sudden changes of chaotic to periodic motion occur. The isoperiodic diagrams, obtained by numerical solution method, corroborate and identify the position of these bifurcation curves, and both reveal the bifurcation structures by period-doubling and by saddle-node in two-dimensional parameter-spaces of the system (1).

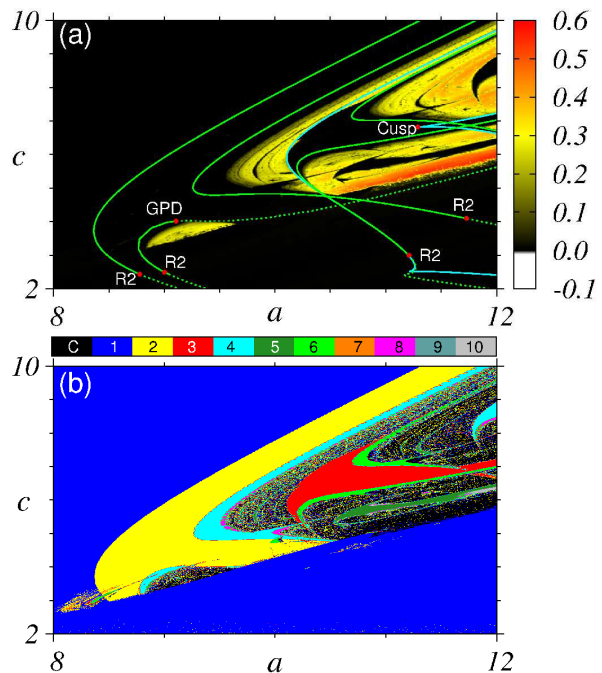


Figure 2: (Color online) In (a) Lyapunov diagram for the  $a \times c$  plane with  $b = 0.55$  and  $d = 10.0$ , for the largest Lyapunov exponent with bifurcation curves superimposed, and in (b) isoperiodic diagram for the same ranges in (a). The top color palette in (b) codifies the periods. Black color codifies chaotic behavior or periods greater than 10.

In Fig. 2(a) we present in more details the period-doubling bifurcation curves, green curves, and the endoskeleton of the period-3 SSD (see the red structure in Fig. 2(b)), *i.e.*, two saddle-node bifurcation curves (cyan curves) with the cusp point in addition with two intersected period-doubling curves (green curves). It is clear to see that these curves delimit regions in the parameter-space that have same periods, as can be observed in Fig. 2(b) (yellow and red domains). In these cases, the curves delimit the domain of lowest period of the SSD's, that is inlaid in the period-1 domain (see the blue region in Fig. 2(b)) and that is immersed in the chaotic domain (see the red structure in Fig. 2(b)). In the Lyapunov diagram of Fig. 2(a) without the bifurcation curves, it is impossible to identify the ingrown SSD of period-2.

Regarding Fig. 3, an amplification of Fig. 1(e), the

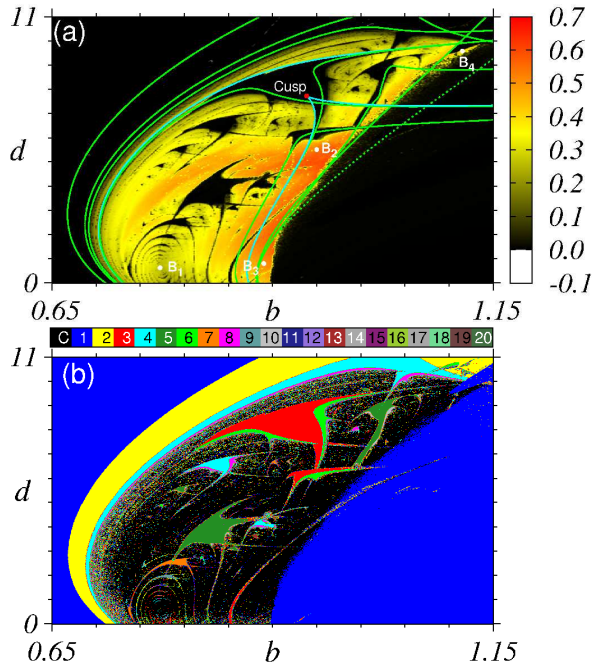


Figure 3: (Color online) In (a) Lyapunov diagram for the  $b \times d$  with  $a = 8.0$  and  $c = 8.5$ , for the largest Lyapunov exponent with bifurcation curves superimposed, and in (b) isoperiodic diagram for the same ranges in (a). The points  $B_1, \dots, B_4$  in (a) will be discussed in Figs. 8 and 9. The top color palette in (b) codifies the periods, in which black color codifies chaotic behavior or periods greater than 20.

same features observed in Fig. 2 is also observed with additional remarks. For instance, in (a) we observe two solid green curves crossing the chaotic domain at right and bordering two distinct periodic structures, the structures of period-3 and 5 in (b), near the period-1 border at right. Inside these structures, the green bifurcation curves delimit the points of period-doubling bifurcation. Indeed, for the period-3 structure (red structure in Fig. 3(b)), the period-doubling bifurcation occurs near the lateral border, corroborating the result shown in Fig. 3(a). The same occurs for the period-5 structure (dark green structure in Fig. 3(b)). The endoskeleton of the bigger period-3 structure in Fig. 3(b) is also clearly visible in Fig. 3(a) with the cusp point inside it.

Other organization structure observed in a two-dimensional parameter-spaces of system (1), is the presence of a periodicity spiral, *i.e.*, self-connected periodic structures that coil up around a focal point. This behavior is shown in Fig. 4, where it is an amplification of Fig. 3. The periodicity spiral was reported in some recent works about three-dimensional Chua's model [20, 29], in other systems [30, 31], and references therein. Here, we show the periodicity spiral

for a four-dimensional Chua's model, and the dimensional parameter  $d$ , that controls the additional dimension of system (1), has a fundamental role in this organization. This organization structure is observed only in parameter-spaces in which the parameter  $d$  is varying, as can be observed in Figs. 1(d)-(f). In Fig. 4(b), we also observe the organization of the periods that increase its value ( $7 \rightarrow 9 \rightarrow 11 \rightarrow 13 \dots$ ) as the structures coil up around a focal point, therefore the bifurcation structure of this spiral follows a period-adding cascade. Bifurcation curves are also superimposed in Fig. 4(a), with period-doubling curves in green and saddle-node curves in cyan. The skeleton of this spiral structure is the connected period-doubling and saddle-node curves. These bifurcation structures of the spiral follow the same structure reported earlier for three-dimensional continuous-time models [17, 20, 28–30] and maps [32].

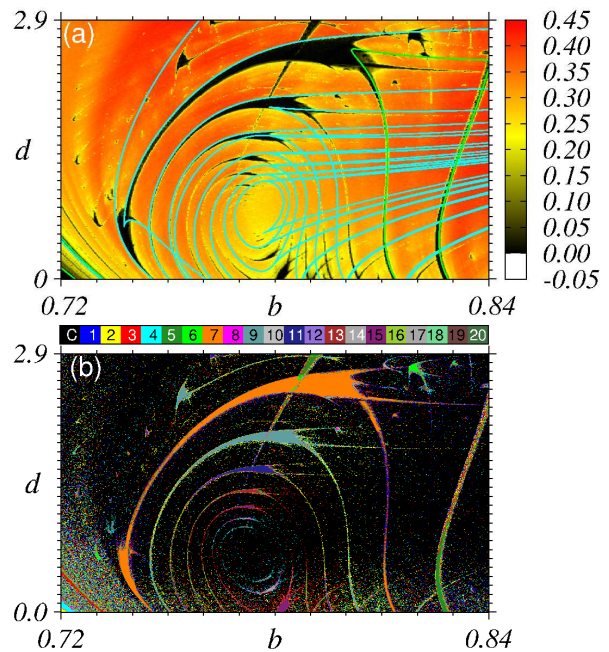


Figure 4: (Color online) Amplification of Fig. 3 emphasizing the periodicity spiral of SSD's. In (a) the Lyapunov diagram, and (b) the isoperiodic diagram, in which black color codifies chaotic behavior or periods greater than 20. Some bifurcation curves are superimposed in the Lyapunov diagram in (a). Green for period-doubling and cyan for saddle-node bifurcations.

Previous works [3, 24] report some Lyapunov diagrams for a three- and four-dimensional version of Chua system, both with cubic nonlinearity. In Ref. [24], the three-dimensional Chua system presented a well-known dynamics, with SSD's embedded in all two-dimensional Lyapunov diagrams, self-organizing by

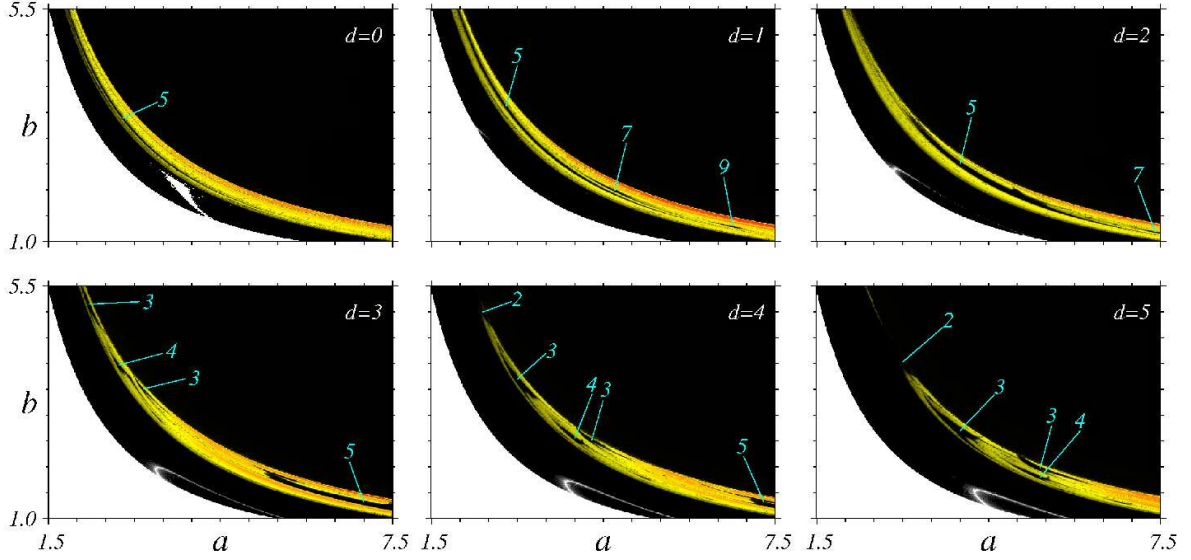


Figure 5: (Color online) Lyapunov diagrams for the  $(a \times b)$  plane with  $c = 12.5$ , for the largest Lyapunov exponent with the parameter  $d$ , whose values are shown in each panel. The cyan numbers are the periods of each structure.

period-adding bifurcation cascades in specific directions in the parameter-spaces, and accumulate in periodic borders. A remarkable difference emerged in the hyperchaotic four-dimensional Chua system reported in Ref. [3], where *malformed*-SSD's become present. This malformation is explained in Ref. [33] using concepts borrowed from the Windows Conjecture [34], that establishes the relation between the branches of the domains near hyperchaotic regions. In few words, the conjecture says that in hyperchaotic systems the branches of the SSD's are limited in the parameter-spaces, in the sense that the branches are broken, and in chaotic systems the branches are extended, *i.e.*, the SSD's extend all over the parameter-spaces. For more details see Refs. [3, 33]. It is worth to mention here, in the set of parameters studied for system (1) and presented in this Letter, we do not observe hyperchaotic behavior, in consequence, all the SSD's present extended branches, as can be observed in Fig. 1. The system (1) presents another interesting feature regarding the dimensional control parameter  $d$ , that is responsible by the coupling of the three-dimensional Chua model with an extra-dimension. To discuss the influence of  $d$ , we show in Fig. 5 the Lyapunov diagrams for six values of  $d$ . For  $d = 0$ , no SSD's is visible on the chaotic domain but there exist just black stripes that indicate periodic domains, however as  $d$  increases the structures appear and become bigger, in addition they present a movement in the chaotic domain as can be observed by their change of position in the diagrams. The plots of Fig. 5 show

how the dynamics change with the dimensional control parameter  $d$  in the system (1). A clear evolution of the SSD's since their births, growths and movements can be observed.

Other interesting feature presented by the system (1) is transient chaos, characterized by topology changes in the attractors after a transient time [35], that is observed in the  $b \times d$  parameter-space. To illustrate this behavior, in Fig. 6 we show the Lyapunov diagrams emphasizing the right period-1 border of Fig. 3. In (a) a transient time of  $5.0 \times 10^5$  was used to evaluate the largest Lyapunov exponent, and in (b) a transient time of  $5.0 \times 10^6$  was used. It is clear to observe the differences between the right black borders in both plots, for example, for  $d$  greater than zero in (a) the border is grained and in (b) the border is sharp. Otherwise, for  $d$  near zero in (a) and (b) the borders are more sharp. To illustrate these features we show in Fig. 7 the changes of chaotic to periodic behavior for two points in Fig. 6(a), namely  $P_1$  and  $P_2$  points, respectively.

In the left column of Fig. 7, (a), (c), and (e), we show the time series for the parameters  $(b, d) = (0.898, 0.1)$  (see the point  $P_1$  in Fig. 6(a)). In Fig. 7(c) the time series is an amplification of Fig. 7(a), to show clearly the change of chaotic to periodic behavior. In Fig. 7(e) we present the behavior of the attractor, beginning in chaotic oscillations (see the red lines) and shortly passing to periodic oscillations (see the green lines). In the right column of Fig. 7, (b), (d), and (f), the time series is for  $(b, d) = (1.05, 8.0)$  (see the point  $P_2$  in Fig.

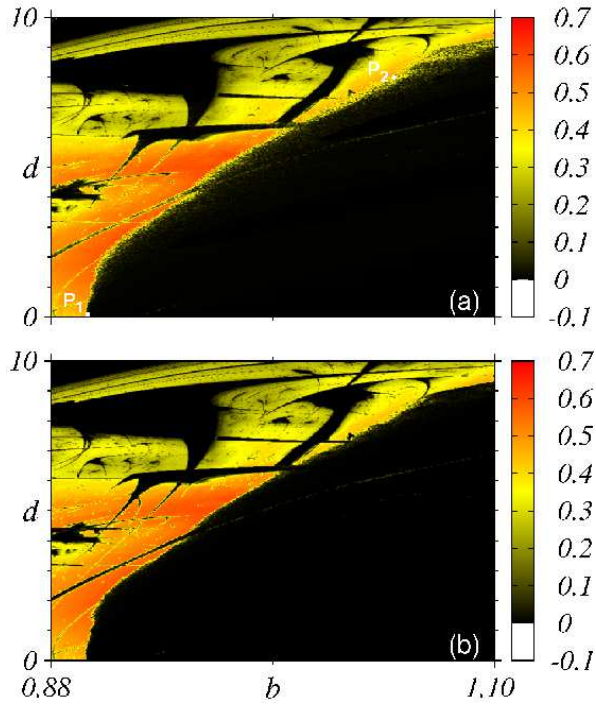


Figure 6: (Color online) Amplification of Fig. 3 emphasizing the right periodic border, in black, where transient chaos is visible. In (a) the transient time is  $5.0 \times 10^5$ , and in (b) is  $5.0 \times 10^6$ .

6(a)). In Fig. 7(d) the time series is an amplification of Fig. 7(b), to show the change between chaotic and periodic behavior. In Fig. 7(f) the attractors are shown. See in more details the chaotic attractors in the insets of Figs. 7(e) and 7(f). In this case, the chaotic oscillations last longer than the previous case (compare the Figs. 7(a) and 7(b)). Following the definitions of the book [35], the two examples presented follow the case in which the nonattracting chaotic set coexists with an asymptotic periodic attractor.

To characterize the role of the initial conditions in the system (1), we investigate the basins of attraction for different sets of parameters. In Figs. 8 and 9 we show some two-dimensional planes of the four-dimensional basins of the points  $B_1, \dots, B_4$  in Fig. 3(a). The basins are obtained by evaluating the largest Lyapunov exponent, and codifying its value with colors. Black color refers to null values and red one refers to positive values, in which is considering a precision of  $10^{-1}$  for positive values. Therefore, black color is the basin for periodic attractors and red is the basin for chaotic attractors. In Fig. 8, the left column presents two planes of the four-dimensional basin of attraction of the  $B_1$  point in Fig. 3(a). This point is the focus of the

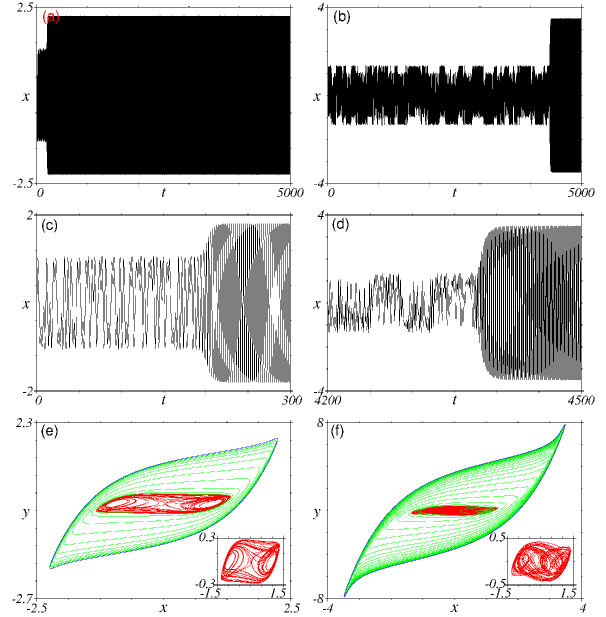


Figure 7: (Color online) Left column, (a),(c), and (e), transient chaos in the point  $P_1$  of Fig. 6(a). Right column, (b), (d), and (f), transient chaos in the point  $P_2$  of Fig. 6(a). In (a)-(d) the time series, and in (e)-(f) the chaotic and periodic attractors with the transient between them. The insets show in more details the chaotic attractors.

spiral structure shown in Fig. 4, roughly estimated at  $(b, d) = (0.773, 0.625)$ . The central column presents the basins for the  $B_2$  point in Fig. 3(a), for the parameters  $(b, d) = (0.95, 5.50)$ , and the right column presents the basins for the  $B_3$  point in Fig. 3(a), for the parameters  $(b, d) = (0.89, 0.80)$ . In Fig. 9 we show the basin of attraction of the  $B_4$  point in Fig. 3(a), for the parameters  $(b, d) = (1.115, 9.57)$ . This point is in the transient chaos region, then the left column in Fig. 9 is for a transient time equal to  $5.0 \times 10^5$ , and the right column is for  $4.5 \times 10^6$ . In both figures it is clear to see that for points closer to the transient chaos region, the basins of attraction are riddled ( $B_3$  and  $B_4$  points), *i.e.*, in the chaotic attractor domain (red region) there exist many black points one referring to the periodic attractor domain, and as the transient time increases the number of black points increases dominating the basin of the chaotic attractor.

#### 4. Conclusions

The dynamics of a four-dimensional Chua system with smooth nonlinearity was studied by numerical continuation and numerical solution methods. By numerical solution methods, the Lyapunov and isoperiodic diagrams, for the largest Lyapunov exponent and for the

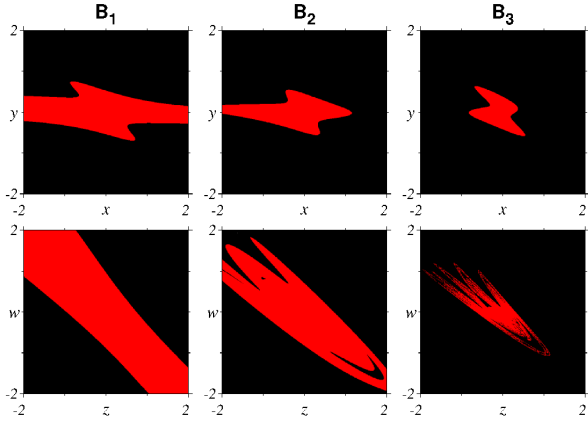


Figure 8: (Color online) Basins of attraction for the points  $B_1$ ,  $B_2$ , and  $B_3$  in Fig. 3(a). Each column shows two-dimensional planes of the four-dimensional basins of these points. For the  $x \times y$  basins,  $(z, w) = (0.1, 0.0)$ , and for the  $z \times w$  basins,  $(x, y) = (0.1, 0.1)$ . Black color is for periodic and red one is for chaotic solutions.

periods, respectively, were used to show how rich is the dynamics presented by the system (1). In addition, by numerical continuation method, Hopf, period-doubling and saddle-node bifurcation curves were constructed to show the bifurcation structures on two-dimensional parameter-spaces.

With the largest Lyapunov exponents, was possible to observe periodic structures immersed in the chaotic regions, and for the parameter  $d$ , that controls the dimension of the system (1), we observed the presence of a periodicity spiral, where periodic structures are connected between them and they coil up around a focal point. This periodicity spiral was observed in three-dimensional continuous-time systems [17, 20, 28–30], recently in a four-dimensional continuous-time system [31], and here we observed in a four-dimensional Chua model. The parameter  $d$  plays another role in system (1) regarding transient chaos. We showed that for  $d$  near zero, the occurrence of transient chaos is small compared with  $d$  greater than zero.

By studying the dynamics in the isoperiodic diagrams we observed two different routes to chaos, at left in the diagrams by period-doubling from periodic region to chaotic one, and at right in the diagrams by crisis from chaotic region to periodic one.

A recent paper [28] proposes a definition of *shrimp*-shaped domain as follows: *Shrimps are formed by a regular set of adjacent windows centered around the main pair of intersecting superstable parabolic arc. A shrimp is a doubly infinite mosaic of stability domains composed by an innermost main domain plus all the adjacent stability domains arising from two period-doubling*

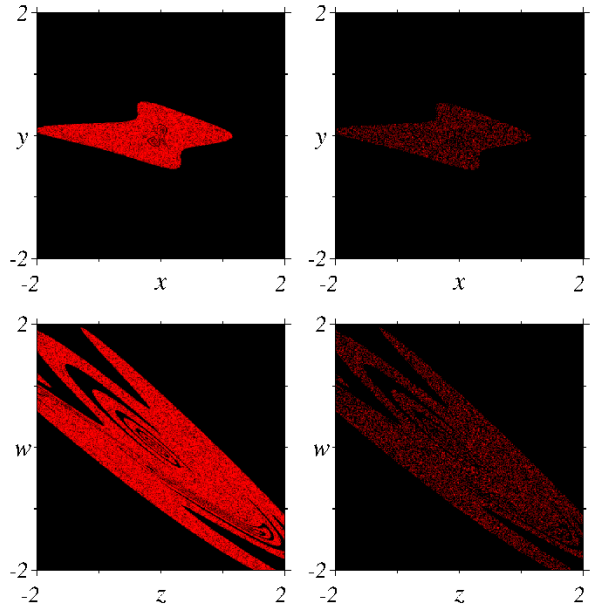


Figure 9: (Color online) Basins of attraction for the point  $B_4$  in Fig. 3(a), in the transient chaos region. Each column shows two-dimensional planes of the four-dimensional basins of this point. The left column is for a transient of  $5.0 \times 10^5$ , and the right column is for a transient of  $4.5 \times 10^6$ . For the  $x \times y$  basins,  $(z, w) = (0.1, 0.0)$ , and for the  $z \times w$  basins,  $(x, y) = (0.1, 0.1)$ . Black color is for periodic and red one is for chaotic solutions.

*cascades together with their corresponding domains of chaos.* In our work the bifurcation curves revealed the endoskeleton of *shrimp*-shaped domains embedded in chaotic regions. The endoskeleton is formed by two saddle-node curves with one cusp point, and two intersected period-doubling curves. The innermost main domain formed by these four curves has the lowest period of the *shrimp*-shaped domain. The period-doubling bifurcation curves showed the existence of a *shrimp*-like domain of period-2 (see Fig. 2) connected to a large period-1 region, and these curves delineate the borders of the lowest period of this structure.

## Acknowledgments

The authors thank CAPES, FAPESC, and CNPq for financial support.

## References

- [1] H. A. Albuquerque, R. M. Rubinger, P. C. Rech, Phys. Lett. A 372 (2008) 4793.
- [2] A. Celestino, C. Manchein, H. A. Albuquerque, M. W. Beims, Phys. Rev. Lett. 106 (2011) 234101.

- [3] C. Stegemann, H. A. Albuquerque, R. M. Rubinger, P. C. Rech, *Chaos* 21 (2011) 033105.
- [4] R. Stoop, S. Martignoli, P. Benner, R. L. Stoop, Y. Uwate, *Int. J. Bifurcation Chaos Appl. Sci. Eng.* 22 (2012) 1230032.
- [5] D. F. M. Oliveira, E. D. Leonel, *Physica A* 392 (2013) 1762.
- [6] D. F. M. Oliveira, E. D. Leonel, *Phys. Lett. A* 376 (2012) 3630.
- [7] E. S. Medeiros, R. O. Medrano-T., I. L. Caldas, S. L. T. D. Souza, *Phys. Lett. A* 377 (2013) 628.
- [8] S. L. T. de Souza, A. A. Lima, I. L. Caldas, R. O. Medrano-T., Z. O. Guimarães-Filho, *Phys. Lett. A* 376 (2012) 1290.
- [9] J. G. Freire, J. A. C. Gallas, *Phys. Lett. A* 375 (2011) 1097.
- [10] W. Façanha, B. Oldeman, L. Glass, *Phys. Lett. A* 377 (2013) 1264.
- [11] R. E. Francke, T. Pöschel, J. A. C. Gallas, *Phys. Rev. E* 87 (2013) 042907.
- [12] C. Manchein, M. W. Beims, *Phys. Lett. A* 377 (2013) 789.
- [13] C. Manchein, A. Celestino, M. W. Beims, *Phys. Rev. Lett.* 110 (2013) 114102.
- [14] A. Celestino, C. Manchein, H. A. Albuquerque, M. W. Beims, *Commun. Nonlinear Sci. Numer. Simul.* 19 (2014) 139.
- [15] P. C. Rech, *Phys. Lett. A* 377 (2013) 1881.
- [16] R. Barrio, F. Blesa, A. Dena, S. Serrano, *Comput. Math. Appl.* 62 (2011) 4140.
- [17] R. Barrio, F. Blesa, S. Serrano, A. Shilnikov, *Phys. Rev. E* 84 (2011) 035201(R).
- [18] A. Ray, D. Ghosh, A. R. Chowdhury, *Phys. Lett. A* 372 (2008) 5329.
- [19] R. Genesio, G. Innocenti, F. Galdani, *Phys. Lett. A* 372 (2008) 1799.
- [20] G. M. Ramirez-Avila, J. A. C. Gallas, *Phys. Lett. A* 375 (2010) 143.
- [21] D. M. Maranhão, M. S. Baptista, J. C. Sartorelli, I. L. Caldas, *Phys. Rev. E* 77 (2008) 037202.
- [22] M. Komuro, R. Tokunaga, T. Matsumoto, L. O. Chua, A. Hotta, *Int. J. Bifurcation Chaos Appl. Sci. Eng.* 01 (1991) 139.
- [23] J. C. D. Cardoso, H. A. Albuquerque, R. M. Rubinger, *Phys. Lett. A* 373 (2009) 2050.
- [24] C. Stegemann, H. A. Albuquerque, P. C. Rech, *Chaos* 20 (2010) 023103.
- [25] L. Liu, C. Liu, Y. Zhang, *Int. J. Bifurcation Chaos Appl. Sci. Eng.* 19 (2009) 2473.
- [26] A. Dhooze, W. Govaerts, Y. A. Kuznetsov, *ACM Trans. Math. Softw.* 29 (2003) 141.
- [27] A. Wolf, J. B. Swift, H. L. Swinney, J. A. Vastano, *Physica D* 16 (1985) 285.
- [28] R. Vitolo, P. Glendinning, J. A. C. Gallas, *Phys. Rev. E* 84 (2011) 016216.
- [29] H. A. Albuquerque, P. C. Rech, *Int. J. Circ. Theor. Appl.* 40 (2012) 189.
- [30] J. Slipantschuk, E. Ullner, M. S. Baptista, M. Zeineddine, M. Thiel, *Chaos* 20 (2010) 045117.
- [31] J. G. Freire, C. Cabeza, A. Marti, T. Pöschel, J. A. C. Gallas, *Sci. Rep.* 3 (2013) 01958.
- [32] P. Gaspard, R. Kapral, G. Nicolis, *J. Stat. Phys.* 35 (1984) 697.
- [33] M. S. Baptista, C. Grebogi, E. Barreto, *Int. J. Bifurcation Chaos Appl. Sci. Eng.* 13 (2003) 2681.
- [34] E. Barreto, B. R. Hunt, C. Grebogi, J. A. Yorke, *Phys. Rev. Lett.* 78 (1997) 4561.
- [35] Y.-C. Lai, T. Tél, *Transient Chaos: Complex Dynamics on Finite Time Scales*, Springer, 2011.